Visualization of instantaneous structure and dynamics of large-scale turbulent flames stabilized by a gliding arc discharge

Gao, Jinlong; Kong, Chengdong; Zhu, Jiajian; Ehn, Andreas; Hurtig, Tomas; Tang, Yong; Chen, Shuang; Aldén, Marcus; Li, Zhongshan

Published in:
Proceedings of the Combustion Institute

DOI:
10.1016/j.proci.2018.06.030

2019

Document Version:
Publisher's PDF, also known as Version of record

Available online at www.sciencedirect.com

ScienceDirect

Proceedings of the Combustion Institute 37 (2019) 5629–5636

Proceedings of the Combustion Institute

www.elsevier.com/locate/proci

Visualization of instantaneous structure and dynamics of large-scale turbulent flames stabilized by a gliding arc discharge

Jinlong Gao [a], Chengdong Kong [a,*], Jiajian Zhu [a], Andreas Ehn [a], Tomas Hurtig [b], Yong Tang [c], Shuang Chen [a], Marcus Aldén [a], Zhongshan Li [a]

[a] *Division of Combustion Physics, Lund University, P.O. Box 118, SE-221 00 Lund, Sweden*
[b] *Swedish Defense Research Agency, SE-164 90 Stockholm, Sweden*
[c] *Key Laboratory for Thermal Science and Power Engineering of Ministry of Education, Department of Energy and Power Engineering, Tsinghua University, Beijing 100084, China*

Received 1 December 2017; accepted 4 June 2018
Available online 22 June 2018

Abstract

A burner design with integrated electrodes was used to couple a gliding arc (GA) discharge to a high-power and large-scale turbulent flame for flame stabilization. Simultaneous OH and CH_2O planar laser-induced fluorescence (PLIF) and CH PLIF measurements were conducted to visualize instantaneous structures of the GA-assisted flame. Six different regions of the GA-assisted flame were resolved by the multi-species PLIF measurements, including the plasma core, the discharge-induced OH region, the post-flame OH region, the flame front, the preheat CH_2O region and the fresh gas mixture. Specifically, the OH profile was observed to be ring-shaped around the gliding arc discharge channel. The formaldehyde (CH_2O) was found to be widely distributed in the entire measurement volume even at a low equivalence ratio of 0.4, which suggest that long-lived species from the gliding arc discharge have induced low-temperature oxidations of CH_4. The CH layer coincides with the interface of the OH and CH_2O regions and indicates that the flame front and the discharge channel are spatially separated by a distance of 3–5 mm. These results reveal that the discharge column acts as a movable pilot flame, providing active radicals and thermal energy to sustain the flame. High-speed video photography was also employed to record the dynamics of the GA-assisted flame. This temporally resolved data was used to study the ignition and propagation behaviors of the flame in response to a temporally

* Corresponding author.
E-mail address: chengdong.kong@forbrf.lth.se (C. Kong).

https://doi.org/10.1016/j.proci.2018.06.030

modulated burst-mode discharge. The results indicate that turbulent flame can be sustained by matching temporal parameters of the high-voltage bursts to the extinction time of flame.

Keywords: Plasma-assisted combustion; Turbulent flame; Gliding arc discharge; PLIF; Flame structure

1. Introduction

Combustion is currently playing a dominant role in energy conversion and transportation. Research of combustion processes and applications mostly focus on how to achieve clean combustion with high efficiency. In the recent decade, plasma, especially the non-thermal plasma has been proposed for combustion enhancement and emission control due to its short response time and multi-effects on combustion through producing active species and heat as well as modifying transport processes [1,2].

Non-thermal plasma can be produced by electric gas discharges. Deposition of electric energy through plasma into a combustion system can generate various radicals and excited species and thus result in new reaction pathways to increase the flame speed and enhance the flame stability. Numerous experiments in laminar flow [3,4] and high-speed turbulent flow [5–7] using radio frequency (RF) plasma [8], gliding arc (GA) discharge [9–11], nanosecond repetitive pulsed discharges [12–14] and microwave discharge [15–17] have shown that the plasma can enhance and stabilize flames. However, it is quite challenging to deposit the energy exactly near the flame zone since the standard flame fronts are thin and spatially inhomogeneous and the electric gas discharge is easily inclined to filamentation at atmospheric pressure or higher [18]. The weak direct interaction between flame and plasma would underestimate the kinetic impacts of plasma. So it is necessary to develop a discharge technique, which can produce a large-volume discharge at high pressure to couple the flame with the plasma efficiently.

In our previous studies, a gliding arc discharge was found to create a non-thermal plasma column, which has a temperature of 1100 K [19] and produces a large amount of radicals (e.g. OH, NO, O_3) [20,21]. The plasma column can propagate together with the flow to increase its interaction time with the surrounding combustible gases. Furthermore, frequent short-cutting events [22] occur to disturb the flow field and enhance mixing. In all, the gliding arc discharge can be a very promising technique to stabilize turbulent flames.

Based upon our understanding of gas discharge (e.g. GA) and turbulent combustion, a burner is designed to couple the gliding arc discharge to a high-power and large-scale turbulent flame for flame stabilization at atmospheric pressure. Different diagnostic techniques including high-speed imaging, current-voltage measurements and OH/CH/CH_2O planar laser induced fluorescence (PLIF) were applied to acquire a detailed description of the GA-assisted combustion system.

2. Experimental setup

Figure 1 shows a schematic of the experimental setup, including the GA-assisted burner and the diagnostic systems. In the homemade burner, the air flow is ejected into a ceramic tube through a 3.8 mm diameter aperture to produce a strong turbulent jet flow, while the methane flows into the reactor tangentially downstream near the orifice of the burner (see the inset of Fig. 1). The air flow rate varies from 50 standard liter per minute (SLM) to 230 SLM, with the mean velocities at the jet exit increasing from 74 m/s to 338 m/s. At a flow rate of 230 SLM, the jet Reynolds number reaches 80,000 and the Kolmogorov length scale can be estimated to be as small as 30 μm assuming a free jet flow [23]. Due to this high-speed jet flow, the flame in the designed burner is highly turbulent and cannot be self-sustained. The gliding arc discharge is formed at the gap between two diverging electrodes inside the ceramic tube and extended up by the flow, as shown in Fig. 1. The two electrodes are internally water-cooled. One of the electrodes is connected to a 35 kHz AC power supply (Generator 9030 E, SOFTAL Electronic GmbH), whereas the other is grounded. The tangential CH_4 jets can generate swirls around the air jet, thus to promote short cuttings of the gliding arc column and broaden the plasma volume.

Different diagnostic techniques were applied to monitor the current/voltage during the discharge and acquire the radical profiles. A current monitor (Pearson Electronics) and a voltage probe (Tektronix P6015A) were employed to measure the waveforms of the current and the voltage simultaneously. A high-speed camera (HSC, Phantom v7.1) equipped with an objective lens (Nikkor 105 mm, f/4) was synchronized to capture the dynamic behaviors of the gliding arc assisted flame.

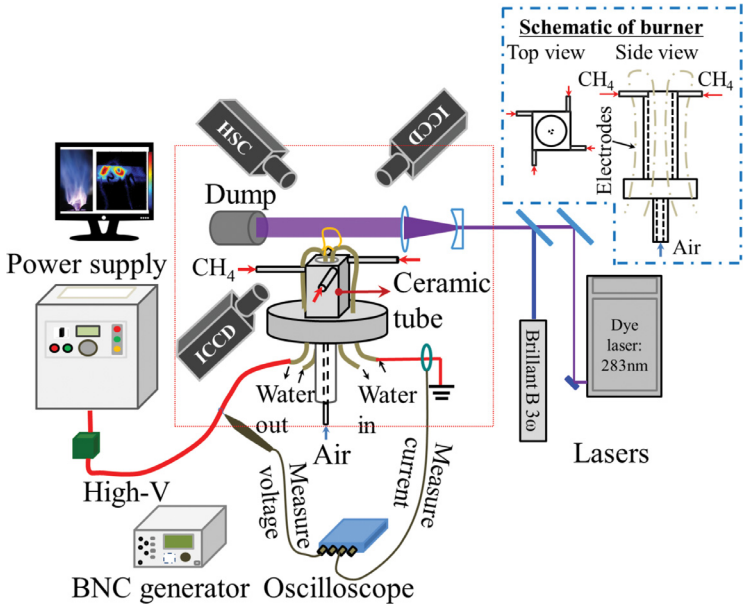

Fig. 1. Schematic of the experimental setup. Inset shows the schematic drawing of the designed burner.

OH and CH_2O PLIF measurements were performed simultaneously to capture the flame structure. A Brilliant B laser with the second and third harmonic units was used to generate a 355 nm laser beam for the excitation of CH_2O [24]. A PIMAX III camera equipped with a visible Nikon lens (105 mm) and a GG395 filter was employed to block the 355 nm laser and collect the fluorescence signal. The laser energy for forming the laser sheet was measured to be around 80 mJ per pulse. The OH PLIF was realized using a Brilliant B pumped dye laser which emits laser beams at a wavelength of 283.55 nm. The Q1 (8) line of the OH transition A-X (1, 0) was probed. A PIMAX II camera with a B-halle lens and an OH filter (Semrock, 320/40) was employed to acquire the OH signal. The two laser beams were spatially combined through a dichroic mirror prior to the sheet-forming optics and synchronized by a BNC pulse generator. The time delay between the two laser beams was set at 100 ns to avoid cross talk. The CH PLIF experiment was conducted using a frequency-doubled Alexandrite laser (101-PAL, Light Age Inc.) at 383.3 nm for the excitation [25]. The current and voltage signals together with the ICCD gates were simultaneously recorded using a four-channel oscilloscope (PicoScope 4424, PS) at a sample rate of 2 GHz.

3. Results and discussion

3.1. Gliding arc sustained turbulent flames

Direct morphologies of the GA-assisted turbulent flames were recorded by a Nikon digital camera (D7200, f/5.6). Figure 2 shows stoichiometric flames supported by the gliding arc discharge with different exposure times. The air flow rate in this case was kept at 230 SLM. Spectral analysis of the spontaneous emission from the discharge supported flame was performed. It indicates that the purple stripes in the photo represent the strong emission from the gliding arc channel while the blue part represents the flame (mainly from the CH emission). Since the emission of the flame is much weaker than that of the arc, the signal from the blue channel of the color images was enhanced for a clearer visualization of flame.

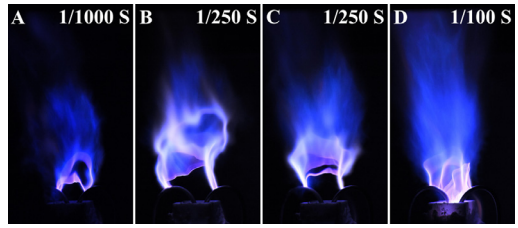

Fig. 2. Direct photos of the stoichiometric turbulent flames assisted by the gliding arc discharge. Exposure time used for different images has been marked out. (For interpretation of the references to color in this figure, the reader is referred to the web version of this article.)

The supporting effect of the gliding arc discharge on the highly turbulent flame is significant. Under high flow rate conditions (230 SLM), the flame will be blown off and cannot be self-sustained. Only when the discharge is present, the

turbulent flame can be held, as shown in Fig. 2A. As we know, the gliding arc discharge column has a translational temperature above 1000 K and full of energetic species [20,21], so the flame is effectively sustained around the discharge column, as shown by the short-exposed photo in Fig. 2A-C. It seems the discharge channel acts as an anchor line to stabilize the flame, with the flame sticking to the discharge channel and propagating downstream. Thus, the flame was observed mostly above the discharge column.

Our previous work has shown that, the gliding arc discharge starts from the narrowest gap between the two electrodes and propagates downstream with the airflow [20,22]. The discharge column can flexibly elongate with the flow to 5 cm and repetitively scan over a large range on account of frequent short-cutting and re-ignition events. This means that the gliding arc discharge can initialize combustion in a volume much larger than the common spark igniters. Therefore, a large-scale turbulent flame is stabilized in this burner, as demonstrated in the long-exposed photo of Fig. 2D. In this experiment, the combustion power of this burner is estimated to be 13 kW by the assumption of complete combustion of the fuel while the rated input power for discharge was set to 0.6 kW. It should be mentioned that the electric input power can be much less than 0.6 kW to sustain the turbulent flame using burst mode by matching temporal parameters of the discharge to the extinction time of flame (see Section 3.3).

3.2. Instantaneous structure of the GA-assisted flame

In the current experimental setup, the turbulent flame at a high flow rate can be stabilized by the gliding arc discharge. The instantaneous structures of the GA-assisted flame were visualized by PLIF images of CH_2O, OH and CH.

3.2.1. Simultaneous OH and CH_2O PLIF profile

Typical simultaneous OH and CH_2O PLIF images at different air flow rates (50 SLM and 230 SLM) are illustrated in Fig. 3. For all the PLIF images shown in this study, the background images recorded without the laser have been subtracted. Due to the strong emission, the discharge channels in the PLIF images are still visible in a string-like shape. Note that the discharge channel moves in three-dimensional space and only parts of the channels cross the laser sheet.

The OH PLIF images are shown in A1 and B1 of Fig. 3. Similar to the observation in our previous work [20], the OH distribution around the discharge channel is ring-shaped with an outer diameter of ~10 mm (marked out with the black dashed curves). The holes in the center of the distributed OH (marked out with dotted lines) identify the plasma core passing through the laser sheet. OH generated from the flame distributes more widely further away from the discharge channel. The OH signal intensity around the channel is 7 times higher than that in the surrounding flames. Usually, OH number density in the flame is on the order of 10^{16} cm^{-3} [26]. If the quenching effect was roughly considered homogenous across the laser sheet, the OH generated by discharge can be estimated to be around 8×10^{16} cm^{-3}. This implies that the discharge volume can produce much more energetic radicals than the flame itself. The influence of equivalence ratio on the OH PLIF signal intensity was also studied. It is found that the OH PLIF intensity around the discharge channel is much higher for the CH_4/air mixture compared with pure air. However, the OH PLIF intensity almost keeps constant with the equivalence ratio increased from 0.4 to 1.

CH_2O PLIF results are shown in A2 and B2 of Fig. 3. Instead of distributed into a thin layer, CH_2O was found spreading into a wide region far away from the discharge channel. CH_2O PLIF measurements were also performed for flames with different equivalence ratios, with the results shown in Fig. 4. Interestingly, the wide distrubiton of CH_2O is detected even for very lean flames with Phi of 0.4 (Fig. 4A), which is beyond the burning limit. Our previous Rayleigh scattering measurment of the translational temperature around the gliding arc indicated that the high temperature region (> 1100 K) is confined in the discharge column with a radius of around 2 mm [19]. Outside this hot region, the temperature drops fast to a value below 900 K. Hence it is speculated that some active species like O_3, generated in the gliding arc discharge, can initiate low-tempeture chemistry of CH_4 to form CH_2O [4,27]. Since CH_2O has a relatively long lifetime, turbulence may also result in the wide spreading of CH_2O. Compared with Fig. 4A, the size of CH_2O region for the stoichometric flame in Fig. 4B becomes smaller. With higher equivalence ratio, the flame initiated from the discharge channel can propagete into further regions, resulting in more CH_2O consumption.

Simultaneous OH and CH_2O PLIF images are overlaid into single images with red and green colors representing OH and CH_2O distributions, respectively, as shown in A3 and B3 of Fig. 3. The overlaid OH and CH_2O PLIF images demonstrate well complementary spatial distribution of OH and CH_2O. CH_2O is usually considered as a marker of the preheat zone, while OH can represent the high-temperature region and active radical pool. Therefore, the interface of these two radicals, OH and CH_2O, indicate the position of the flame front. As illustrated in Fig. 3, the flame front is spatially separated from the plasma core with a gap of 3-5 mm.

3.2.2. CH PLIF profile

CH PLIF technique has been extensively used to visualize the flame front directly in turbulent

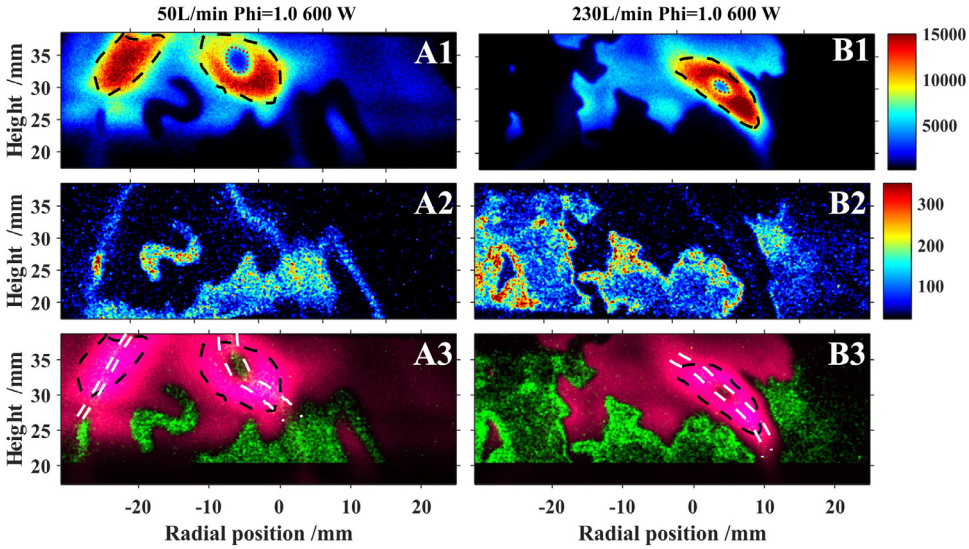

Fig. 3. Simultaneous OH and CH_2O PLIF measurements in the GA-assisted turbulent flame. A1, B1: OH PLIF images; A2, B2: CH_2O PLIF images; A3, B3: overlaid OH & CH_2O PLIF images. Air flow rate in A1 A2 A3:50 SLM; B1 B2 B3: 230 SLM. Equivalence ratio: Phi. (For interpretation of the references to color in this figure, the reader is referred to the web version of this article.)

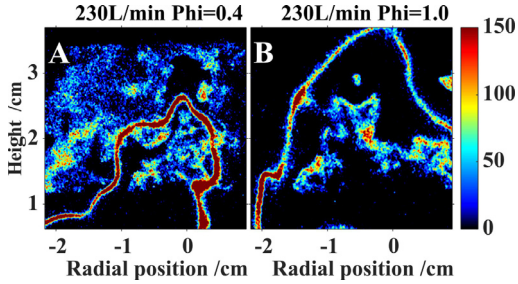

Fig. 4. CH_2O PLIF measurements of the GA-assisted turbulent flame; A: Phi = 0.4, B: Phi = 1.0.

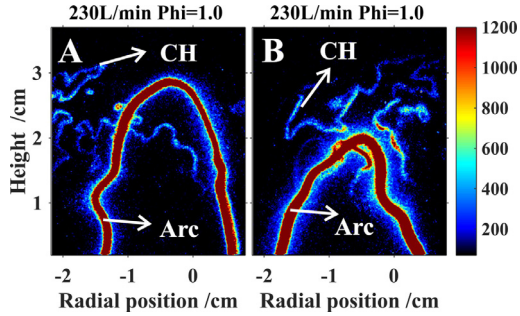

Fig. 5. CH PLIF measurements for the GA-assisted flame with an air flow rate of 230 SLM (Phi = 1.0).

flames. In this study, the CH PLIF technique was employed to reveal the distribution of flame fronts relative to the discharge channel. Some typical CH PLIF images are shown in Fig. 5. For the CH PLIF measurements, only a long-pass filter (GG400) was used to block the 383 nm laser scattering and thus the strong arc emissions (marked with arrow in Fig. 5) were detected together with the CH layer in the short-gated images. Similar to conventional turbulent flames, the CH signal distributes into a thin layer (less than 1 mm in thickness) and wrinkles due to the turbulent flow. The flame front indicated by the CH layer has a gap to the discharge channel. This gap is several millimeters wide, that is consistent with the estimate from the simultaneous OH & CH_2O PLIF measurements.

3.2.3. Discussion on the structure of GA-assisted flame

According to the multi-species PLIF measurements, a schematic of the GA-assisted flame structure is illustrated by the inset S in Fig. 6. The gliding arc channel, or the plasma core, where free electrons pass through and most excited or ionized species are located, situates in the most inner part, as shown by white dash lines in A3 and B3 of Fig. 3.

Around the plasma core, there is a region featured with energetic species like OH. OH in this region is induced by the gliding arc discharge and has higher concentration than that generated in the flame, as indicated by the black dash curves in Fig. 3A and 3B. Since the active radical species are influenced by the plasma core, this region can

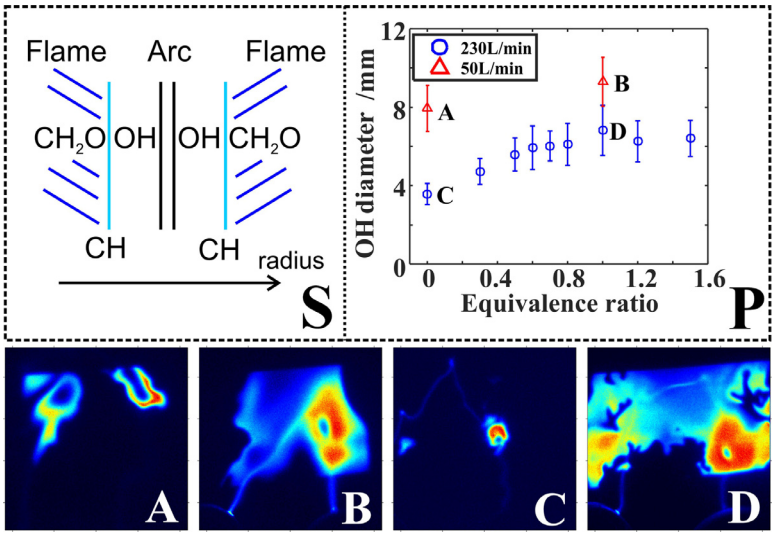

Fig. 6. S: schematic of the structure of GA-assisted flame. P: Diameters of OH region induced by the gliding arc discharge at different equivalence ratios and different air flow rates. A-D: Single-shot OH PLIF images: A: 50 SLM, Phi = 0; B: 50 SLM, Phi = 1; C: 230 SLM, Phi = 0; D: 230 SLM, Phi = 1.

represent the active volume of the gliding arc discharge. Beyond the discharge-induced OH region, the remaining OH signal in the OH PLIF images (Figs. 3A 3B 6B and 6D) refers to the post-flame region. OH signal in this region is relatively weak and distributes more widely towards downstream. Outside the OH region is the preheat region, which is filled with CH_2O. It is speculated that some long-lived species like O_3 contribute to the low temperature oxidation of CH_4 into intermediates like CH_2O. This low-temperature oxidation of fuel can enhance the flame ignition and stabilization [27]. The interface between the CH_2O and OH regions, i.e. the CH layer characterizes the flame front, represented by the blue lines in Fig. 6S.

The influence of Phi on the size of the discharge-induced OH region is shown in Fig. 6P. The effective diameters of discharge-induced OH region (marked with black curve in Fig. 3A and 3B) were measured based on the OH PLIF images. Without the CH_4 addition, there is already OH appeared since the electrons in the discharge channel can dissociate the water vapor in the air. With the increment of air flow rate from 50 SLM to 230 SLM, the diameter of the OH ring decreases from about 8 mm (Fig. 6A) to 4 mm (Fig. 6C). When CH_4 is added, the OH diameter at an air flow rate of 230 SLM is still smaller than that at an air flow rate of 50 SLM, yet the difference becomes less, as illustrated by inset B and D. For an air flow rate of 230 SLM, the increase of CH_4 content steadily enlarges the OH distribution from 4 mm to around 7 mm with Phi varying from 0 to 1.0. When Phi is beyond 1.0, the diameter of the OH ring does not increase any more with the equivalence ratio. It implies some interaction of discharge and combustion.

Diameter of the discharge-induced OH region is mainly dominated by the dissipation of OH. High flow rate can promote the turbulent mixing to accelerate the OH dissipation and thereby reduce its diameter. Combustion can further provide a high-temperature environment to shield the discharge column and reduce the loss of OH. This shielding effect is a reason for the smaller difference of OH diameters at air flow rates of 50 SLM and 230 SLM with CH_4 added (see Fig. 6B and 6D).

3.3. *Dynamics of the GA-assisted flame propagation*

A high speed camera was used to record the dynamical behavior of the GA-assisted flame. The flame propagations at the air flow rate of 230 SLM was recorded and shown in Fig. 7. The high speed video was synchronized with the current-voltage measurements. The instantaneous current-voltage values corresponding to the high speed video frames have been marked out by arrow with numbers in Fig. 7. A proper threshold was used to distinguish the discharge channel from the flame. The flame area was shown in green color while the discharge channel was shown in red. Owing to the heat and active radicals provided by the discharge, the flame can be started by the discharge efficiently as demonstrated in Frame 1 of Fig. 7. After the initiation of the combustion (Frame 1), the

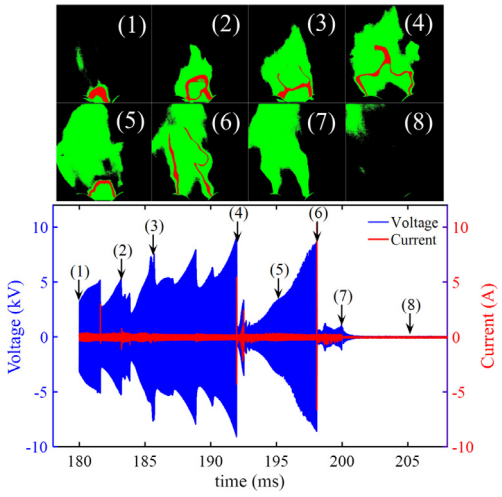

Fig. 7. High speed images of the GA-assisted flame (plasma column is in red and the flame is in green), together with the simultaneously recorded current and voltage waveforms. Air flow rate is 230 SLM and Phi is 0.7. The frame rate of the high speed camera is 5000 Hz. (For interpretation of the references to color in this figure legend, the reader is referred to the web version of this article.)

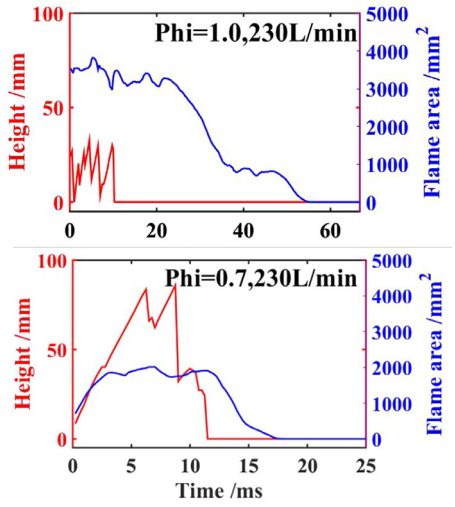

Fig. 8. Variation of the flame area and the height of the gliding arc with respect to time with different equivalent ratios. The blue curve shows the temporal evolution of the flame area while the red curve show the height of the gliding arc discharge. (For interpretation of the references to color in this figure legend, the reader is referred to the web version of this article.)

flame propagates together with the gliding arc. The flame area increases with elongation of the discharge channel from Frame 1 to Frame 4. At the time of 200 ms (Frame 7), the power supply to the gliding discharge was switched off. Hereafter, the discharge channel disappears and the flame is blown out since the turbulent flame speed is lower than the flow speed (Frame 8). Meanwhile, the flame begins to extinct due to the turbulent dissipation of heat and radicals.

The extinction time of flame is dependent on the local chemical kinetics and flow field. So the influence of the equivalence ratio on the extinction time was examined. The results are plotted in Fig. 8, where the blue curve shows the temporal evolution of the flame area (measured from a series of high-speed video images) while the red curve shows the height of the discharge column. At a given flow rate, the extinction time of stoichiometric flames is measured to be about 35 ms longer than that of the lean flames.

The power supply for discharge can be set to the burst mode, which means the high voltage is imposed on the electrode for a time period and off for another time period, alternately, as shown by the blue curve in Fig. 9. The delay time between high-voltage bursts were varied from 3 ms to 30 ms. When the delay time is large (e.g 30 ms), the flame will totally blow out during the delay. Fig. 9 actually reflects the extinction time of flame. For the case (i.e. 230 SLM and Phi = 1) the mean extinc-

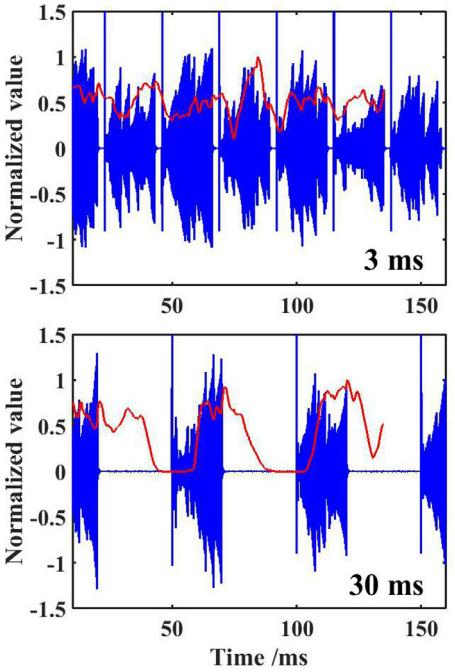

Fig. 9. Temporal evolutions of voltage and the relative flame area. The blue line is the voltage (normalized by 10 kV) and the red one is the relative flame area (normalized by the peak area). (For interpretation of the references to color in this figure legend, the reader is referred to the web version of this article.)

tion time is around 10-20 ms. If the delay time is as short as 3 ms, the flame can be sustained without overall blown out. Therefore, turbulent combustion can be continuously sustained by the burst-mode discharges. Furthermore, if the power supply is modulated to match the extinction time of flame, the average discharge power can be much reduced.

4. Summary

Gliding arc discharge transforms the input electrical energy into heat and energetic species. The high temperature and energetic species provided by the discharge can effectively initiate the combustion process even under highly turbulent and lean conditions. With the support of gliding arc discharge, a large-scale turbulent flame with a power of 13 kW was sustained in our designed burner.

The instantaneous structure of this GA-assisted flame was visualized by multi-species PLIF diagnostic tools. Accordingly, six regions can be divided from the plasma core to surrounding fresh gas mixtures, including the plasma core, the discharge-induced OH region, the post-flame OH region, the flame front, the preheat CH_2O region and the fresh gas mixture. The average diameter of discharge-induced OH regions is around 6 mm, which means the active discharge column for flame holding is larger than the visible discharge channel (~1 mm). The simultaneous OH & CH_2O PLIF measurements indicate that the flame front is 3-5 mm away from the discharge channel. The wide spread of CH_2O at an equivalence ratio of 0.4 suggests a low-temperature chemistry of CH_4. It seems some long-lived radicals from the plasma column can oxidize the fuel to CH_2O, which has a higher burning velocity and is beneficial for the flame stabilization.

High speed video photography was employed to study the response of the turbulent flame to the gliding arc discharge. The discharge channel can ignite the flame effectively, after which the turbulent flame propagates downstream. When the discharge is shut off, the flame can still sustain for tens of milliseconds before extinction. The extinction time is dependent on the local chemical composition and the flow field. The typical extinction time of stoichiometric flame at an air flow rate of 230 SLM is around 10–20 ms. Modulating the power supply in burst mode according to the extinction time can minimize the input energy of discharge to sustain the turbulent flame.

Generally, we demonstrate that in our setup a large discharge volume can be coupled to turbulent flames, which enable a prompt ignition and stabilization of large-scale turbulent flames efficiently. In view of the availability of gliding arc discharge in high turbulent conditions, it will be an effective approach to sustain large-scale turbulent lean flames.

Acknowledgement

The work was financially supported by the Swedish Energy Agency, the Swedish Research Council, the Knut and Alice Wallenberg foundation, the European Research Council and the National Natural Science Foundation of China (No. 51606217).

References

[1] A. Starikovskiy, N. Aleksandrov, *Prog. Energ. Combust.* 39 (2013) 61–110.
[2] Y. Ju, W. Sun, *Prog. Energ. Combust.* 48 (2015) 21–83.
[3] V.E. Kozlov, A.M. Starik, N.S. Titova, *Combust. Explos. Shock Waves* 44 (2008) 371–379.
[4] W. Weng, E. Nilsson, A. Ehn, et al., *Combust. Flame* 162 (2015) 1284–1293.
[5] A. Ehn, J. Zhu, P. Petersson, et al., *Proc. Combust. Inst.* 35 (2015) 3487–3495.
[6] S.B. Leonov, D.A. Yarantsev, *Plasma Sources Sci. Technol.* 16 (2007) 132–138.
[7] H. Do, S.K. Im, M.A. Cappelli, M.G. Mungal, *Combust. Flame* 157 (2010) 2298–2305.
[8] B.C. Thelen, D. Chun, E. Toulson, T. Lee, IEEE Trans. Plasma Sci., 41 (2013) 3223–3232.
[9] T. Ombrello, X. Qin, Y. Ju, A. Gutsol, A. Fridman, C. Carter, *AIAA J.* 44 (2006) 142–150.
[10] D.H. Lee, K.-T. Kim, M.S. Cha, Y.-H. Song, *Proc. Combust. Inst.* 31 (2007) 3343–3351.
[11] T. Ombrello, Y. Ju, A. Fridman, *AIAA J.* 46 (2008) 2424–2433.
[12] M.S. Bak, H. Do, M.G. Mungal, M.A. Cappelli, *Combust. Flame* 159 (2012) 3128–3137.
[13] S. Nagaraja, V. Yang, Z.Y. Yin, I. Adamovich, *Combust. Flame* 161 (2014) 1026–1037.
[14] W. Sun, S.H. Won, T. Ombrello, C. Carter, Y. Ju, *Proc. Combust. Inst.* 34 (2013) 847–855.
[15] A. Ehn, P. Petersson, J. Zhu, et al., *Proc. Combust. Inst.* 36 (2017) 4121–4128.
[16] E.S. Stockman, S.H. Zaidi, R.B. Miles, C.D. Carter, M.D. Ryan, *Combust. Flame* 156 (2009) 1453–1461.
[17] X. Rao, K. Hemawan, I. Wichman, et al., *Proc. Combust. Inst.* 33 (2011) 3233–3240.
[18] S.M. Starikovskaia, *J. Phys. D Appl. Phys.* 47 (2014) 353001–353034.
[19] J. Zhu, A. Ehn, J. Gao, et al., *Opt. Express* 25 (2017) 20243–20257.
[20] J. Zhu, Z. Sun, Z. Li, et al., *J. Phys. D Appl. Phys.* 47 (2014) 295203.
[21] Z. Sun, J. Zhu, Z. Li, et al., *Opt. Express* 21 (2013) 6028–6044.
[22] J. Zhu, J. Gao, A. Ehn, et al., *Phys. Plasmas* 24 (2017) 013514.
[23] B. Zhou, C. Brackmann, Q. Li, et al., *Combust. Flame* 162 (2015) 2937–2953.
[24] C. Brackmann, J. Nygren, X. Bai, et al., *Spectro-chim. Acta A* 59 (2003) 3347–3356.
[25] Z. Li, J. Kiefer, J. Zetterberg, et al., *Proc. Combust. Inst.* 31 (2007) 727–735.
[26] Z.Y. Yin, C.D. Carter, W.R. Lempert, *Appl. Phys. B* 117 (2014) 707–721.
[27] Y. Ju, J.K. Lefkowitz, C.B. Reuter, et al., *Plasma Chem. Plasma Process* 36 (2016) 85–105.